GEOMORPHOLOGY

Experimental evidence for hillslope control of landscape scale

K. E. Sweeney,[1]* J. J. Roering,[1] C. Ellis[2]

Landscape evolution theory suggests that climate sets the scale of landscape dissection by modulating the competition between diffusive processes that sculpt convex hillslopes and advective processes that carve concave valleys. However, the link between the relative dominance of hillslope and valley transport processes and landscape scale is difficult to demonstrate in natural landscapes due to the episodic nature of erosion. Here, we report results from laboratory experiments combining diffusive and advective processes in an eroding landscape. We demonstrate that rainsplash-driven disturbances in our experiments are a robust proxy for hillslope transport, such that increasing hillslope transport efficiency decreases drainage density. Our experimental results demonstrate how the coupling of climate-driven hillslope- and valley-forming processes, such as bioturbation and runoff, dictates the scale of eroding landscapes.

Convex hillslopes and concave valleys are ubiquitous in eroding, soil-mantled landscapes (*1*–*3*) (Fig. 1, A and B). These distinct landforms are produced by equally distinct sediment transport processes: On hillslopes, abiotic (*4*, *5*) and biotic (*6*, *7*) disturbance agents disperse sediment downslope, whereas in valleys, sediment is transported by debris flows (*8*) or flowing water (*9*). The transition between hillslopes and valleys has long been considered a fundamental landscape scale (*3*, *10*, *11*), but there is debate over what controls its style and position. Numerical results suggest that the hillslope-valley transition may be dictated by the minimum runoff necessary for sediment detachment or landslide initiation (*11*–*13*) or by the competition between diffusive transport on hillslopes and advective transport in channels (*14*, *15*).

These geomorphic models predict expansion or contraction of the valley network from changes in climatic variables such as precipitation and vegetation (*3*, *12*, *16*). Hence, rigorous testing of controls on the hillslope-valley transition is central to our understanding of landscape response to environmental perturbations. Due to the slow and episodic nature of erosion, however, field tests are limited to comparisons of steady-state model predictions with natural topography [e.g., (*2*)]. Such approaches rely on the assumption that topography reflects long-term average fluxes, ignoring the potentially important effects of initial conditions (*17*) and temporal lags between landscape response and climatic and tectonic forcing (*18*, *19*).

We conducted a series of laboratory experiments to determine whether the competition between hillslope transport and valley incision sets the spatial scale of landscapes (*15*). The theoretical underpinnings of the process control on the hillslope-valley transition derive from a statement of mass conservation, where the rate of elevation change (dz/dt) is equal to uplift rate (U), minus erosion due to disturbance-driven hillslope diffusion and channel advection by surface runoff

$$\frac{\partial z}{\partial t} = U + D\nabla^2 z - K(PA)^m S^n \qquad (1)$$

where D is hillslope diffusivity, K is the stream power constant, A is drainage area, S is slope, P is precipitation rate (assuming steady, uniform rainfall), and m and n are positive constants (*9*). In this framework, the strength of hillslope transport relative to channel processes can be quantified by the landscape Péclet number (Pe), assuming $n = 1$ (*15*)

$$Pe = \frac{KL^{2m+1}}{D} \qquad (2)$$

where L is a horizontal length scale and the hillslope-valley transition occurs at the critical length scale L_c where $Pe = 1$ (*15*). In plots of slope versus drainage area, L_c corresponds to a local maximum separating convex hillslope and concave valley topography (*20*) (Fig. 1, D and E). If this framework holds for field-scale and experimental landscapes, increasing the vigor of hillslope transport relative to valley incision (decreasing Pe) should result in longer hillslopes (higher L_c)

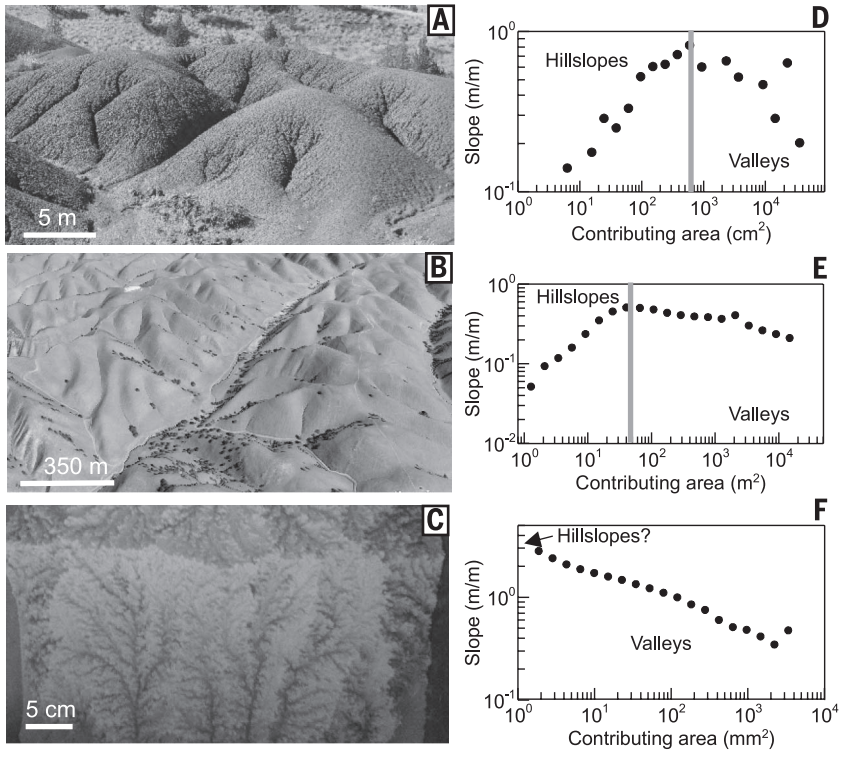

Fig. 1. Characteristic morphology of eroding landscapes. Photographs of eroding landscapes. (**A**) Painted Hills unit of John Day Fossil Beds National Monument, Oregon. (**B**) Gabilan Mesa, California. (**C**) Laboratory landscape from this study with no hillslope diffusion, and associated plots of local slope versus drainage area, calculated with steepest descent algorithm (**D** to **F**). Pictures in (A) and (C) taken by the author (K.E.S.); (B) from Google Earth. Topographic data to generate slope-area plots from (D) field surveys; (E) Lidar data from National Center for Airborne Laser Mapping; and (F) this study. Gray vertical bars in (D) to (F) demarcate the inferred hillslope-valley transition (*34*).

[1]Department of Geological Sciences, University of Oregon, 1272 University of Oregon, Eugene, OR 97403-1272, USA. [2]St. Anthony Falls Laboratory and National Center for Earth-Surface Dynamics, College of Science and Engineering, University of Minnesota, 2 Third Avenue SE, Minneapolis, MN 55414-2125, USA.
*Corresponding author. E-mail: kristin.e.sweeney@gmail.com

and a contraction of the valley network (i.e., a decrease in drainage density).

Experimental landscapes bridge the gap in complexity between numerical models and natural landscapes (*21*) by enabling us to control the confounding influences of tectonics, climate, and lithology and observe surface evolution through time. As previously noted [e.g., (*21*)], a complete dynamical scaling of erosional landscapes in the laboratory is typically intractable due to shallow water depths, large grain sizes relative to the size of the experiment, and other considerations. Nonetheless, past landscape experiments have successfully demonstrated the topographic manifestation of changing uplift rate (*22*, *23*), precipitation rate (*24*), and precipitation patterns (*25*). In these experiments, however, erosion was exclusively driven by surface runoff (e.g., Fig. 1, C and F), intentionally excluding the representation of diffusive hillslope processes (*22*) and hence precluding tests for the role of hillslope transport in setting landscape scale.

Following Eq. 1, we created an experimental system that distilled landscape evolution into three essential ingredients: base-level fall (uplift), surface runoff (channel advection), and sediment disturbance via rainsplash (hillslope diffusion) (Fig. 2). Our experiments in the eXperimental Landscape Model (XLM) at the St. Anthony Falls Laboratory systematically varied the strength of disturbance-driven transport relative to surface runoff (changing *Pe*) for steady, uniform uplift. The XLM consists of a 0.5 by 0.5 by 0.3 m^3 flume with two parallel sliding walls, each connected to a voltage-controlled dc motor to simulate relative uplift (Fig. 2A). The experimental substrate was crystalline silica (median grain size = 30 μm) mixed with 33% water to increase cohesion and reduce infiltration (Fig. 2C). We began each experiment by filling the XLM with sediment and allowing it to settle for ~24 hours to homogenize moisture content. Topographic data at 0.5 mm vertical accuracy were collected at regular time intervals on a 0.5 by 0.5 mm grid using a laser scanner.

Sediment transport in our experiments was driven by two distinct rainfall systems: the mister, a rotating ring fitted with 42 misting nozzles, and the drip box, a polyvinyl chloride constant head tank fitted with 625 blunt needles of 0.3 mm interior diameter arranged in a 2 by 2 cm grid (Fig. 2B). The fine drops produced by the mister lack sufficient energy to disturb sediment on impact and instead result only in surface runoff. By contrast, the 2.8 mm diameter drops from the drip box are sufficiently energetic to create rainsplash and craters on the experiment surface that result in sediment transport. We used four fans mounted on the corners of the experiment to generate turbulence and randomize drop location during drip box rainfall. Importantly, sediment transport due to drip box rainfall consists of both hillslope diffusion from the cumulative effect of drop impacts and nonnegligible advective transport due to the subsequent runoff of the drops. Thus, we expect that changing the relative contribution of rainsplash results in a change in both hillslope and channel transport efficiency (*D* and *K*, respectively).

We ran five experiments, varying the time of drip box rainfall (i.e., predominantly diffusive transport) from 0 to 100% of total experiment runtime (Fig. 3 and table S1) (*26*) and holding base-level fall and water flux from the mister and the drip box constant. During the experiment, we alternated between drip box rainfall and mister rainfall over 10-min periods (table S1); the fans used for drip box rainfall prevented simultaneous operation. We continued each experiment until we reached flux steady state such that the spatially averaged erosion rate was equal to the rate of base-level fall (figs S1 and S2). Each experiment ran for 10 to 15 hours, encompassing 60 to 90 intervals of drip box and/or mister rainfall.

The steady-state topography of our experiments (Fig. 3, A to F) demonstrates how increasing the relative dominance of rainsplash disturbance affects landscape morphology. Qualitatively, landscapes formed by a higher percentage of drip box rainfall (Fig. 3E) appear smoother, with wider, more broadly spaced valleys and extensive unchannelized areas. In contrast, landscapes with more surface runoff transport (Fig. 3A), equivalent to past experimental landscapes (*24*, *27*), are

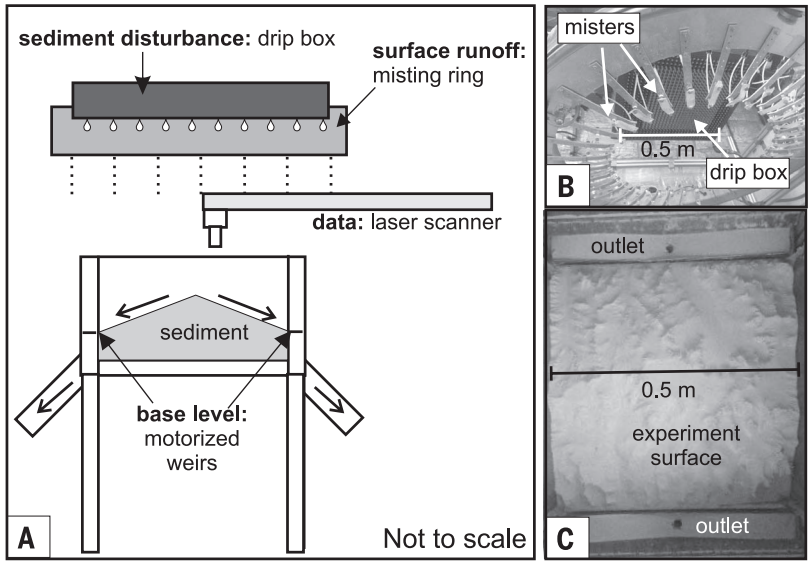

Fig. 2. Experimental setup. (**A**) Schematic profile of experimental apparatus (XLM). Line arrows show direction of sediment movement. (**B**) Photograph of misting ring and drip box looking from below. (**C**) Photograph of sediment surface during 100% drip run.

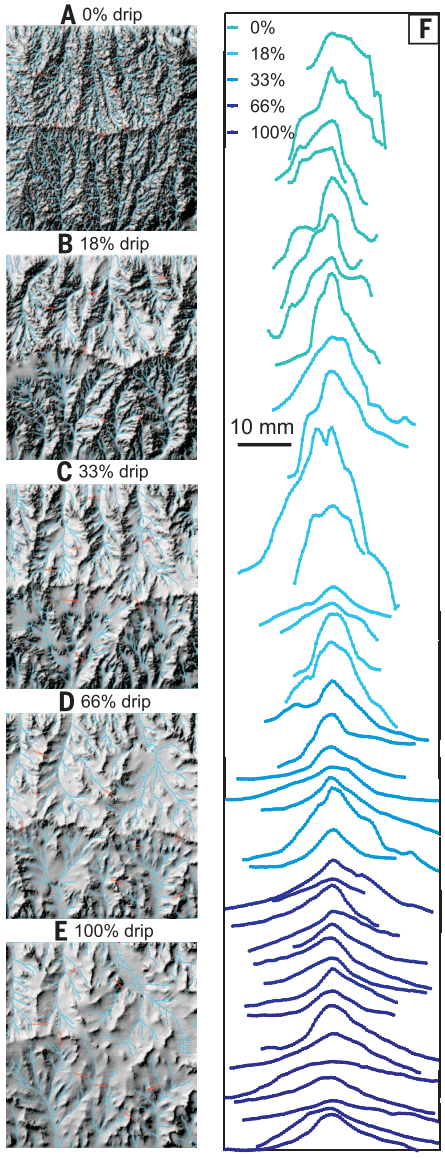

Fig. 3. Steady-state topography and hillslope morphology. (**A** to **E**) Hillshades of experimental topography for (A) 0% drip, (B) 18% drip, (C) 33% drip, (D) 66% drip, and (E) 100% drip overlain with channel networks (blue) and locations of hillslope profiles (red). Topography is 475.5 mm wide in planview. (**F**) Elevation profiles of hillslopes marked by red lines in (A) to (E). Vertical and horizontal length scales are equal.

densely dissected. As the relative percentage of rainsplash increases, hillslope transects increase in both length and topographic curvature (Fig. 3F), confirming that our experimental procedure can be used to adjust hillslope transport efficiency. Hillslope relief in our experiments is approximately 10 to 20% of total landscape relief, a similar value to natural landscapes (*28*).

To test the expected relationship between Péclet number and landscape scale (*15*) (Eq. 2), we used steady-state relationships between landscape morphology and sediment transport laws to independently calculate D and K. This approach is often not possible in natural landscapes and thus extends our theoretical understanding beyond the slope-area plots shown in Fig. 1, D to F. Specifically, we used the approach of (*28*) to calculate D, which uses average hillslope length and gradient, thereby avoiding the stochastic imprint of individual raindrop impacts that can obscure local metrics of hillslope form, such as curvature. The following relationship relates mean hillslope gradient ($\overline{S}$) to hillslope length (L_h), critical slope (S_c), erosion rate (E, equal to U at steady state), and hillslope diffusivity (D)

$$\frac{\overline{S}}{S_c} = \frac{1}{E^*}\left(\sqrt{1+(E^*)^2} - \ln\left(\frac{1}{2}\left[1+\sqrt{1+(E^*)^2}\right]\right) - 1\right) \quad (3)$$

where $E^* = E(2L_h/KS)$ (*28*). To calculate K and m for the stream power model, we used the prediction of Eq. 1 that local steady-state channel slope is a power-law function of drainage area (*29*):

$$S = \left(\frac{U}{KP^m}\right)^{\frac{1}{n}} A^{-m/n} \quad (4)$$

To quantify hillslope length and gradient, we mapped the channel network by explicitly identifying channel forms (*28*–*31*) (fig. S3), then traced hillslopes beginning at hilltop pixels by following paths of steepest descent to the nearest channel (*28*) (fig. S3). We take S_c to be sufficiently large (table S1) that Eq. 3 approximates linear diffusion. As the proportion of rainsplash transport increases, D calculated from Eq. 3 also increases (table S1), confirming that the morphologic trend of individual hillslope transects (Fig. 3F) reflects increasing hillslope transport efficiency.

To calculate the advective process parameters (Eq. 4), we extracted slope and steepest-descent drainage area data along networks defined by a minimum drainage area of 250 mm^2 (larger than the drainage area of channel initiation) and fit power-law relationships to plots of slope versus drainage area (*29*). Following (*15*, *22*), we assume that $n = 1$ and use the intercept and slope of the power-law fits to calculate m and K for each experiment. Whereas m is relatively invariant for all our experiments, K tends to increase with the fraction of drip box transport, indicating that post-impact rainfall runoff contributes to advective as well as diffusive transport in our experiments.

Given that both D and K change in our experiments, we calculated Pe values (Eq. 2) for each of our experiments to quantify how diffusive and advective processes contribute to the observed transition from smooth and weakly channelized landscapes (100% drip box, Fig. 3A) to highly dissected terrain (mist only, 0% drip box, Fig. 3E). We calculated Pe for each experiment (Eq. 2) by assuming that $n = 1$ and taking the length scale L to be the horizontal distance from the main divide to the outlet (256 mm). Our results show that landscape Pe value increases with the fraction of drip box transport, demonstrating that an increase in hillslope transport efficiency, D, is the dominant result of increasing rainsplash frequency. Figure 4 reveals a positive relationship between Pe and drainage density, which is inversely related to hillslope length or L_c, such that increasing Pe in our experiments results in higher drainage density (i.e., shorter hillslopes). This finding is consistent with theoretical predictions for coupled hillslope-channel process controls on the scale of landscape dissection (*14*, *15*).

In our experiments, hillslope transport imparts a first-order control on landscape scale, emphasizing the need to establish functional relationships between climate variables and hillslope process rates and mechanisms for real landscapes. Although climate change scenarios typically focus on the influence of vegetation and rainfall on overland flow and channel hydraulics (*3*, *12*), climate controls on the vigor of hillslope transport (e.g., *32*, *33*) can drive changes in landscape form. Robust linkages between transport processes and topography, as discussed here, are an important component of interpreting planetary surfaces as well as decoding paleolandscapes and sedimentary deposits.

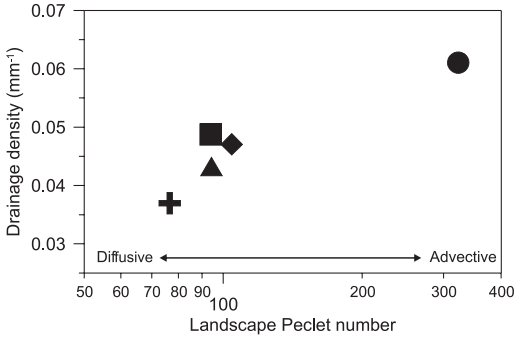

Fig. 4. Effect of landscape Péclet number on landscape scale. Landscape Péclet number for each experiment (circle, 0% drip; square, 18% drip; diamond, 33% drip; triangle, 66% drip; plus sign, 100% drip) versus drainage density of GeoNet-derived drainage networks.

REFERENCES AND NOTES

1. W. M. Davis, *Science* **20**, 245 (1892).
2. G. K. Gilbert, *J. Geol.* **17**, 344–350 (1909).
3. G. Moglen, E. Eltahir, R. Bras, *Water Resour. Res.* **34**, 855–862 (1998).
4. N. Matsuoka, *Permafr. Periglac. Process.* **9**, 121–133 (1998).
5. D. J. Furbish, K. K. Hamner, M. W. Schmeeckle, M. N. Borosund, S. M. Mudd, *J. Geophys. Res.* **112** (F1), F01001 (2007).
6. E. J. Gabet, *Earth Surf. Process. Landf.* **25**, 1419–1428 (2000).
7. J. J. Roering, J. Marshall, A. M. Booth, M. Mort, Q. Jin, *Earth Planet. Sci. Lett.* **298**, 183–190 (2010).
8. J. Stock, W. E. Dietrich, *Water Resour. Res.* **39**, n/a (2003).
9. A. D. Howard, *Water Resour. Res.* **30**, 2261–2285 (1994).
10. M. J. Kirkby, *Spec. Publ. Inst. Br. Geogr.* **3**, 15–30 (1971).
11. D. Montgomery, W. Dietrich, *Water Resour. Res.* **25**, 1907–1918 (1989).
12. A. Rinaldo, W. E. Dietrich, R. Rigon, G. K. Vogel, I. Rodrlguez-Iturbe, *Nature* **374**, 632–635 (1995).
13. R. Horton, *Geol. Soc. Am. Bull.* **56**, 275–370 (1945).
14. T. R. Smith, F. P. Bretherton, *Water Resour. Res.* **8**, 1506–1529 (1972).
15. J. T. Perron, J. W. Kirchner, W. E. Dietrich, *Nature* **460**, 502–505 (2009).
16. G. E. Tucker, R. Slingerland, *Water Resour. Res.* **33**, 2031–2047 (1997).
17. J. Taylor Perron, S. Fagherazzi, *Earth Surf. Process. Landf.* **37**, 52–63 (2012).
18. K. Whipple, G. E. Tucker, *J. Geophys. Res.* **104** (B8), 17661–17674 (1999).
19. J. J. Roering, J. W. Kirchner, W. E. Dietrich, *J. Geophys. Res.* **106** (B8), 16499–16513 (2001).
20. J. T. Perron, W. E. Dietrich, J. W. Kirchner, *J. Geophys. Res.* **113** (F4), F04016 (2008).
21. C. Paola, K. Straub, D. Mohrig, L. Reinhardt, *Earth Sci. Rev.* **97**, 1–43 (2009).
22. D. Lague, A. Crave, P. Davy, *J. Geophys. Res.* **108** (B1), 2008 (2003).
23. J. M. Turowski, D. Lague, A. Crave, N. Hovius, *J. Geophys. Res.* **111** (F3), F03008 (2006).
24. S. Bonnet, A. Crave, *Geology* **31**, 123 (2003).
25. S. Bonnet, *Nat. Geosci.* **2**, 766–771 (2009).
26. Materials and methods are available as supplementary material on *Science* Online.
27. L. Hasbargen, C. Paola, *Geology* **28**, 1067 (2000).
28. J. J. Roering, J. T. Perron, J. W. Kirchner, *Earth Planet. Sci. Lett.* **264**, 245–258 (2007).
29. C. Wobus *et al.*, in *Tectonics, Climate, and Landscape Evolution: Geological Society of America Special Paper 398*, S. D. Willett, N. Hovius, M. T. Brandon, D. M. Fisher, Eds. (Geological Society of America, Boulder, CO, 2006), pp. 55–74.
30. M. D. Hurst, S. M. Mudd, R. Walcott, M. Attal, K. Yoo, *J. Geophys. Res.* **117** (F2), F02017 (2012).
31. P. Passalacqua, T. Do Trung, E. Foufoula-Georgiou, G. Sapiro, W. E. Dietrich, *J. Geophys. Res.* **115** (F1), F01002 (2010).
32. J. L. Dixon, A. M. Heimsath, J. Kaste, R. Amundson, *Geology* **37**, 975–978 (2009).
33. O. A. Chadwick *et al.*, *Geology* **41**, 1171–1174 (2013).
34. W. Dietrich, C. Wilson, D. Montgomery, J. McKean, R. Bauer, *Geology* **20**, 675–679 (1992).

ACKNOWLEDGMENTS

This work was supported by a National Science Foundation grant (EAR 1252177) to J.J.R. and C.E. We thank D. Furbish and A. Singh for fruitful discussions, S. Grieve and M. Hurst for assistance with the calculation of hillslope metrics, and the technical staff of St. Anthony Falls Laboratory for support during experiments. All authors designed the experiments and wrote the manuscript, C.E. built and troubleshot the experimental apparatus, and K.E.S. conducted the experiments and analyzed the data. Comments from two anonymous reviewers greatly improved the manuscript. Topographic data are available from the National Center for Earth Dynamics Data Repository at https://repository.nced.umn.edu.

SUPPLEMENTARY MATERIALS

www.sciencemag.org/content/349/6243/51/suppl/DC1
Materials and Methods
Figs. S1 to S3
Table S1
References (*35*)

3 March 2015; accepted 26 May 2015
10.1126/science.aab0017

Experimental evidence for hillslope control of landscape scale
K. E. Sweeney *et al.*
Science **349**, 51 (2015);
DOI: 10.1126/science.aab0017